Research Square

Preprints are preliminary reports that have not undergone peer review.
They should not be considered conclusive, used to inform clinical practice,
or referenced by the media as validated information.

Non-invasive nomogram predicting moderate-severe renal interstitial fibrosis and tubular atrophy integrating biochemical markers and ASL-MRI histogram features in chronic kidney disease

Xiuzhen Liang[1]

2298993816@qq.com

Ningbo Medical Center Lihuili Hospital

Mingjie Wu[1]

Ningbo Medical Center Lihuili Hospital

Zhibing Liu[1]

Ningbo Medical Center Lihuili Hospital

Xupeng Shen[1]

Ningbo Medical Center Lihuili Hospital

Xueyan Gan[1]

Ningbo Medical Center Lihuili Hospital

Article

Keywords: chronic kidney disease, renal interstitial fibrosis, arterial spin labeling MRI, histogram analysis, predictive nomogram

Posted Date: November 11th, 2026

DOI: https://doi.org/10.21203/rs.3.rs-10944100/v1

License: This work is licensed under a Creative Commons Attribution 4.0 International License.
Read Full License

Additional Declarations: No competing interests reported.

Abstract

Objective This study aimed to construct a non-invasive predictive model for renal interstitial fibrosis and tubular atrophy (IFTA) in patients with chronic kidney disease (CKD) by integrating clinical biochemical indicators and histogram features derived from arterial spin-labeling magnetic resonance imaging (ASL-MRI), and to evaluate its diagnostic performance and clinical translational value.

Methods A prospective cohort of 98 CKD patients undergoing renal biopsy and 3.0T three-dimensional pseudo-continuous arterial spin-labeling (3D-pCASL) examination between November 2024 and May 2026 were enrolled. Patients were divided into mild IFTA group (n = 61) and moderate-severe IFTA group (n = 37) according to pathological IFTA grading. Clinical biochemical markers including serum creatinine (Scr) and estimated glomerular filtration rate (eGFR) were collected. Mean renal cortical perfusion and 17 histogram parameters from ASL-MRI were extracted. Univariate analysis and least absolute shrinkage and selection operator (Lasso) regression were used to screen predictive factors, followed by collinearity assessment before building a multivariate logistic regression combined model. Two comparator models (biochemical-only model and ASL mean perfusion-only model) were built simultaneously. Receiver operating characteristic (ROC) curve, 1000-time bootstrap internal validation, decision curve analysis (DCA), and eGFR-stratified subgroup analysis were performed for comprehensive model evaluation.

Results Univariate analysis revealed inter-group differences in Scr, eGFR, blood urea nitrogen, serum uric acid, 24-hour urinary protein (24hUP), and 13 ASL histogram parameters. Lasso regression retained five core predictors: Scr, eGFR, 24hUP, Median and TotalEnergy. Variance inflation factor (VIF) < 5 for all variables indicated no severe multicollinearity. Multivariate logistic regression showed that only 24hUP was an independent risk factor for moderate-severe IFTA. The AUC was 0.737 for the ASL mean perfusion-only model, 0.904 for the biochemical-only model, and 0.946 for the combined multi-modal model. Delong test showed the combined model outperformed the ASL mean perfusion-only model significantly ($P < 0.001$), whereas the AUC improvement compared with biochemical-only model was not statistically significant ($P = 0.092$). After 1000-bootstrap internal validation, the corrected AUC reached 0.921; Hosmer-Lemeshow test $P = 0.845$ indicated good calibration. DCA demonstrated favorable net clinical benefit across risk thresholds. Subgroup analysis showed stable performance with AUC = 0.919 in patients with eGFR ≥ 60 mL/min/1.73 m² and AUC = 0.985 in patients with eGFR < 60 mL/min/1.73 m². A nomogram was plotted for individualized risk estimation of moderate-severe IFTA.

Conclusion ASL-MRI histogram analysis quantifies heterogeneous renal cortical perfusion and compensates limitations of single mean perfusion metrics for focal parenchymal injury detection. The multi-modal combined model integrating biochemical markers and ASL histogram features achieves good discriminative power, favourable calibration and stable subgroup performance, showing promising potential for risk stratification and longitudinal follow-up in CKD patients, although the incremental diagnostic value added by ASL-MRI histogram features did not reach statistical significance compared with biochemical markers alone.

1 Introduction

Chronic kidney disease (CKD) has evolved into a major global public health burden with rising incidence and disease-related socioeconomic costs. Renal interstitial fibrosis and tubular atrophy (IFTA) represents the shared pathological pathway and core driver of progression to end-stage kidney disease (ESKD) across all etiologies of CKD[1–2]. The severity of IFTA directly determines the rate of renal function decline and long-term clinical prognosis. Early, precise and non-invasive evaluation of IFTA is critical for individualized clinical intervention and risk stratification.Renal biopsy remains the diagnostic gold standard for IFTA grading[3–4]. However, this invasive procedure carries risks of hemorrhage and other complications, restricting its application in mass population screening, serial dynamic monitoring and therapeutic efficacy evaluation. Conventional clinical biochemical indicators exhibit limited sensitivity for early occult interstitial renal fibrosis and significant time lag, failing to satisfy current clinical diagnostic demands[5–6].

Arterial spin labeling magnetic resonance imaging (ASL-MRI) allows non-invasive quantitative measurement of renal cortical perfusion without exogenous gadolinium contrast agents, enabling early detection of microcirculatory impairment secondary to renal fibrosis with favorable safety and repeatability[7]. Further histogram analysis of ASL perfusion maps quantifies the heterogeneous distribution of renal parenchymal perfusion, capturing microstructural alterations induced by focal IFTA lesions, which provides richer pathological information than single mean perfusion values and substantially improves diagnostic performance[8].

Nevertheless, existing predictive models for renal fibrosis possess notable drawbacks: most models only incorporate biochemical markers or isolated imaging features without effective multi-dimensional information fusion; multicollinearity among high-dimensional features is rarely fully addressed, impairing model stability and generalizability; subgroup stratified validation is generally absent, restricting clinical translational potential[9–10].

To address these gaps, this study constructed a non-invasive predictive model for IFTA by integrating routine biochemical markers and ASL-MRI histogram features, with feature optimization via Lasso regression. The established model provides an accurate, generalizable quantitative non-invasive tool for early evaluation of interstitial fibrosis in CKD populations.

2 Materials and Methods

2.1 Study Population

We prospectively enrolled 98 CKD patients admitted to the nephrology department between November 2024 and May 2026, who completed both renal biopsy and standardized 3.0T ASL-MRI scanning. Inclusion criteria:(1)Diagnosis of CKD consistent with international KDIGO criteria[11];(2)Completion of 3.0T 3D-pCASL kidney MRI within 1 week prior to renal biopsy, with image quality meeting the

requirements of renal cortical ROI delineation and histogram parameter extraction;(3)Complete pathological specimens obtained from renal biopsy to perform standardized semi-quantitative IFTA grading. Exclusion criteria:(1)Concurrent acute kidney injury, rapidly progressive glomerulonephritis, urinary tract infection, obstructive nephropathy and other acute renal lesions;(2)Contraindications to MRI examination (metallic implants, claustrophobia, pregnancy, etc.);(3)Severe concurrent cardiac, hepatic or respiratory failure precluding renal biopsy;(4)Severe renal siderosis or intrarenal hemorrhage.

This prospective study was approved by the Institutional Review Board of our hospital (Approval No. 2024-IRB-434), and informed consent was waived by the ethics committee.

2.2 Data Collection

2.2.1 Clinical Biochemical Data

Baseline clinical laboratory parameters were extracted, including age, serum creatinine (Scr), estimated glomerular filtration rate (eGFR), blood urea nitrogen (BUN), serum uric acid (UA), and 24-hour urinary protein quantification (24hUP).

2.2.2 ASL-MRI Acquisition Protocol

All subjects underwent renal MRI examinations on a Philips Ingenia Elition X 3.0T scanner equipped with a 16-channel phased-array abdominal coil. Routine renal morphological sequences and three-dimensional pseudo-continuous arterial spin labeling (3D-pCASL) were acquired with respiratory gating compensation. Key scanning parameters: TR = 4033 ms, TE = 16 ms, slice thickness = 8 mm, slice gap = 0 mm, flip angle = 90°, NEX = 1, FOV = 280 mm × 262 mm, matrix = 76 × 60; labeling offset distance = 90 mm, post-label delay (PLD) = 1800 ms. Background suppression and M0 reference images were acquired simultaneously, with built-in motion correction algorithms applied. Renal blood flow (RBF) was automatically quantified by the scanner workstation based on a single-compartment kinetic model[12]:$RBF=[60 \times \lambda \times (SIcontrol - SIlabel) \times \exp(-PLD/T1blood)]/[2 \times SIM0 \times T1blood \times (1 - \exp(-2\tau/T1blood))]$; T1blood = 1664 ms at 3.0T; SIcontrol/SIlabel represent signal intensity of control/label images; SIM0 denotes baseline reference signal; τ indicates labeling duration. Standardized RBF maps were exported after automatic correction.

2.2.3 Image Post-processing and Histogram Feature Extraction

All image analyses were independently performed by two radiologists with ≥ 5 years of abdominal imaging experience under double-blinded conditions.(1)Mean cortical RBF measurement: At standard renal hilar slice, three circular ROIs (10 mm² each) were drawn in anterior, middle and posterior renal cortex, avoiding renal sinus, large vessels and focal lesions; the average value of three ROIs was recorded as mean ASL perfusion(Fig. 1).(2)ASL histogram feature extraction: Denoised perfusion maps were imported into 3D Slicer software for batch extraction of 17 cortical histogram parameters. Inter-

observer reproducibility was assessed via intraclass correlation coefficient (ICC); only features with ICC > 0.85 were retained for subsequent analysis.

2.2.4 Pathological IFTA Grading Standard

Renal biopsy slides were double-blindly reviewed by two renal pathologists with ≥ 10 years of diagnostic experience, integrating light microscopy, immunofluorescence and electron microscopy results. Patients were dichotomized according to international semi-quantitative criteria[13]: mild IFTA group (interstitial fibrosis involving 0%–25% cortical area) and moderate-severe IFTA group (fibrosis area > 25%). IFTA severity was treated as a binary outcome variable (0 = mild, 1 = moderate-severe) for logistic regression modeling.

2.3 Statistical Analysis

Statistical analyses were conducted using SPSS 26.0 and R 4.3.0 software. Two-tailed $P < 0.05$ was defined as statistically significant; Bonferroni correction was applied for multiple intergroup comparisons.

1. **2.3.1 Univariate intergroup comparison**: Continuous variables were presented as mean ± standard deviation. Independent sample t-test (Welch's correction for unequal variance) was used for between-group comparisons of biochemical indicators and ASL histogram parameters. Variables with statistically significant intergroup differences were selected as candidate predictive features.
2. **2.3.2 Lasso-Logistic feature selection**: Binary IFTA status was set as the dependent variable, with candidate features as independent predictors. Penalized Lasso logistic regression (glmnet package) with 10-fold cross-validation was used to identify the optimal λ.min penalty coefficient; variables with non-zero regression coefficients were retained as core predictors. All continuous predictors were Z-score standardized to eliminate dimensional differences.
3. **2.3.3 Multicollinearity diagnosis**: Pearson correlation heatmap visualization and variance inflation factor (VIF) quantification were combined to assess collinearity; VIF ≥ 5 indicated severe multicollinearity.
4. **2.3.4 Multivariate logistic regression and nomogram construction**: Selected predictors were incorporated into binary multivariate logistic regression to calculate standardized β coefficients, odds ratios (OR) and corresponding 95% confidence intervals (CI); a forest plot was generated for visualization. A predictive nomogram was established via the rms package to realize rapid individualized risk estimation of moderate-severe IFTA.
5. **2.3.5 Discriminative performance evaluation**: Three predictive models were constructed for head-to-head comparison: Model 1 (combined model: biochemical markers + ASL histogram features + mean ASL perfusion), Model 2 (biochemical-only model), Model 3 (mean ASL perfusion-only model). ROC curves were plotted to calculate AUC, sensitivity and specificity; Delong test was used to pairwise compare AUC values and quantify incremental diagnostic gain from histogram features.
6. **2.3.6 Model calibration assessment**: 1000-time bootstrap resampling was performed to generate calibration curves, comparing model-predicted probability against actual pathological IFTA

prevalence. Hosmer-Lemeshow goodness-of-fit test (P > 0.05 represented satisfactory calibration without systematic bias).

7. **2.3.7 Decision curve analysis (DCA)**: DCA was plotted to quantify standardized net clinical benefit across different risk thresholds, evaluating the clinical application value of the model.
8. **2.3.8 Subgroup validation stratified by eGFR**: The entire cohort was split into two subgroups at eGFR = 60 mL/min/1.73m², with AUC recalculated in each stratum to verify model stability across different renal function stages.

3 Results

3.1 Baseline Biochemical Characteristics Between Two Groups

A total of 98 CKD patients were enrolled, including 61 patients with mild IFTA and 37 patients with moderate-severe IFTA. No significant intergroup difference in age was observed (P = 0.683). Scr, eGFR, BUN, UA and 24hUP all exhibited statistically significant differences between groups (Table 1).

Table 1
Baseline biochemical characteristics of patients stratified by IFTA severity

Index	Age	Scr (μmol/L)	eGFR (mL/min/1.73m²)	BUN (mmol/L)	UA (μmol/L)	24hUP (mg/24h)
Mild IFTA (n = 61)	40.43 ± 12.63	80.52 ± 22.15	94.79 ± 23.80	5.83 ± 1.43	346.41 ± 85.62	1134.33 ± 1076.79
Moderate-severe IFTA (n = 37)	41.49 ± 12.04	143.71 ± 53.30	53.11 ± 20.36	8.13 ± 2.87	399.51 ± 82.00	2576.87 ± 2715.10
t-value	-0.41	-6.86	9.21	-4.54	-3.02	-3.09
P-value	0.68	<0.05	<0.05	<0.05	<0.05	<0.05

3.2 Intergroup Comparison of ASL Histogram Parameters

After t-test and Bonferroni multiple testing correction (α = 0.002778), 13 out of 17 histogram parameters showed significant intergroup differences, including 10Percentile, 90Percentile, Energy, Entropy, InterquartileR, MeanAD, Mean, Median, Range, RobustMAD, RootMS, TotalEnergy and Uniformity. Kurtosis, Maximum, Minimum, Skewness and Variance displayed no statistical difference post-correction and were excluded from candidate features (Table 2).

Table 2
Intergroup comparison of ASL cortical histogram parameters

Texture Feature	Mild Group	Moderate-Severe Group	t value	P value	After Bonferroni Correction
10Percentile	833 ± 171	717 ± 184	3.17	0.002	significant
90Percentile	2189 ± 642	1711 ± 556	3.76	<0.001	significant
Energy	$1.01\times10^{12}\pm7.02\times10^{11}$	$4.99\times10^{11}\pm3.86\times10^{11}$	4.62	<0.001	significant
Entropy	6.01 ± 0.54	5.59 ± 0.54	3.74	<0.001	significant
InterquartileR	798 ± 329	549 ± 315	3.68	<0.001	significant
Kurtosis	2.52 ± 0.45	2.99 ± 1.20	-2.74	0.007	not significant
Maximum	2654 ± 749	2194 ± 690	3.04	0.003	not significant
MeanAD	432 ± 167	315 ± 156	3.44	<0.001	significant
Mean	1496 ± 362	1210 ± 324	3.93	<0.001	significant
Median	1486 ± 342	1210 ± 325	3.94	<0.001	significant
Minimum	123 ± 145	219 ± 218	-2.39	0.020	not significant
Range	2531 ± 791	1974 ± 776	3.40	0.001	significant
RobustMAD	322 ± 133	226 ± 125	3.55	<0.001	significant
RootMS	1586 ± 402	1274 ± 359	3.86	<0.001	significant
Skewness	-0.09 ± 0.23	0.02 ± 0.45	-1.56	0.121	not significant
TotalEnergy	$3.83\times10^{13}\pm2.68\times10^{13}$	$1.87\times10^{13}\pm1.50\times10^{13}$	4.64	<0.001	significant
Uniformity	0.019 ± 0.009	0.026 ± 0.009	-3.63	<0.001	significant
Variance	307018 ± 215982	182713 ± 191168	2.88	0.005	not significant

3.3 Predictive Factor Selection via Lasso Regression

Five predictors with non-zero regression coefficients were retained at optimal λ.min penalty: Scr, 24hUP, Median, TotalEnergy and eGFR. Standardized regression coefficients were listed as follows: TotalEnergy = -0.49, Median = -0.12, Scr = 1.21, 24hUP = 1.18, eGFR = -1.02. Scr and 24hUP represented risk factors for moderate-severe IFTA (positive coefficients), while eGFR, Median and TotalEnergy served as protective factors (negative coefficients) (Fig. 2).

3.4 Multicollinearity Diagnosis

VIF values of all enrolled predictors were below 5: eGFR = 4.81, Median = 4.52, TotalEnergy = 4.18, Scr = 4.05, mean ASL perfusion = 2.26, 24hUP = 1.17, without severe multicollinearity. Pearson correlation heatmap revealed strong negative correlation between Scr and eGFR (r=-0.85), strong positive correlation between Median and TotalEnergy (r = 0.84); correlation coefficients between other features were moderate or weak, with controllable collinearity risk (Fig. 3).

3.5 Multivariate Binary Logistic Regression Results

Six standardized features were incorporated into multivariate logistic regression. Only 24hUP was identified as an independent risk factor for moderate-severe IFTA (β = 1.598, OR = 4.943, 95%CI: 1.849–13.215, P = 0.001). Scr, Median, eGFR, mean ASL perfusion and TotalEnergy exhibited P > 0.05 without independent predictive effect, yet joint inclusion significantly improved overall discriminative efficacy of the integrated model (Fig. 4). A visualized predictive nomogram was constructed based on regression coefficients to calculate personalized probability of moderate-severe IFTA by summing the point score of each predictor (Fig. 5).

3.6 Comparative Discriminative Efficacy of Three Predictive Models

Biochemical-only model (Scr + eGFR): AUC = 0.904 (95%CI: 0.841–0.967), sensitivity = 75.7%, specificity = 96.7%;Mean ASL perfusion-only model: AUC = 0.737 (95%CI: 0.638–0.836), sensitivity = 73.0%, specificity = 72.1%;Combined multi-modal model (biochemistry + ASL histogram + mean perfusion): AUC = 0.946 (95%CI: 0.906–0.985), sensitivity = 78.4%, specificity = 95.1%;

Delong test results:Biochemical-only model was significantly superior to mean ASL perfusion-only model (Z = 2.79, P = 0.005);Combined multi-modal model outperformed mean ASL perfusion-only model significantly (Z = 4.19, P < 0.001);The combined model displayed numerically higher AUC than biochemical-only model without statistical intergroup difference (Z = 1.68, P = 0.092), indicating modest incremental diagnostic value introduced by ASL histogram features (Fig. 6).

3.7 Model Calibration, Bootstrap Validation and DCA

After 1000-time bootstrap internal validation, the bias-corrected AUC of the combined model was 0.921, with minimal optimism bias of 0.025, indicating negligible overfitting risk. Hosmer-Lemeshow test χ^2 = 4.14, df = 8, P = 0.845 > 0.05, with calibration curve closely fitting the ideal diagonal line, demonstrating excellent model calibration. DCA demonstrated that the combined model yielded higher standardized net clinical benefit than "treat all" and "treat none" reference strategies across the full risk threshold range of 0.01–0.99, supporting broad clinical applicability for outpatient risk stratification (Fig. 7).

3.8 Subgroup Stability Stratified by eGFR

Stratified analysis at eGFR cutoff 60 mL/min/1.73m² verified robust performance of the integrated model across different renal function stages:Subgroup eGFR ≥ 60 (n = 67, IFTA positive n = 11): AUC = 0.919 (95%CI: 0.846–0.992), sensitivity = 100%, specificity = 76.8% at optimal cutoff;Subgroup eGFR < 60 (n = 31, IFTA positive n = 26): AUC = 0.985 (95%CI: 0.948–1.000), sensitivity = 92.3%, specificity = 100% at optimal cutoff.No obvious decline in discriminative performance was observed in either subgroup, confirming consistent reliable IFTA discrimination across the full spectrum of CKD renal impairment severity.

4 Discussion

IFTA represents the irreversible pathological driver of CKD progression to ESKD[14–15], and developing non-invasive, repeatable quantitative assessment tools for IFTA remains a hotspot in nephrogenic quantitative imaging research. This study constructed a fully validated multi-modal predictive model integrating routine biochemistry, mean ASL perfusion and ASL histogram texture features, with systematic methodological optimization to overcome limitations of existing predictive models. Key findings are elaborated from multiple dimensions as below:

4.1 ASL Histogram Texture Quantifies Focal Heterogeneous Renal Injury

Mean renal blood flow derived from ASL-MRI can evaluate IFTA in CKD patients, yet most prior studies only adopted single global mean perfusion values with evident diagnostic limitations[16–17]. A previous single-center prospective study demonstrated[18] that mean ASL RBF only achieved an AUC of 0.827 for distinguishing early CKD patients with normal eGFR from healthy controls, consistent with our result of AUC = 0.737 for the perfusion-only model. Pathologically, IFTA lesions distribute heterogeneously and focally in renal parenchyma; MRI histogram parameters correlate closely with peritubular capillary density and capture microstructural heterogeneity missed by averaged perfusion metrics[19]. In our study, 13 histogram parameters exhibited significant intergroup differences after multiple testing correction, and Lasso regression filtered Median and TotalEnergy as core imaging predictors. Lower Median and TotalEnergy values were observed in moderate-severe IFTA patients, consistent with previous pathological and imaging reports. By integrating histogram texture with biochemical markers, the combined model elevated AUC from 0.904 (biochemical alone) to 0.946, with statistically significant improvement compared to single perfusion parameter, validating the incremental diagnostic gain of histogram heterogeneity quantification.Of note, although the combined model had a numerically higher overall AUC than the biochemical-only model, the difference was not statistically significant (P = 0.092). The added value of ASL histogram features was mainly reflected in maintaining stable diagnostic performance among patients with preserved renal function (eGFR ≥ 60 mL/min/1.73 m²).

4.2 Multi-modal Fusion Compensates Temporal Limitations of Single Biochemical Markers

Most published IFTA predictive models solely rely on serum biochemical indicators, which suffer from inherent methodological defects. The kidney possesses substantial functional reserve capacity[20–22], microvascular rarefaction and focal collagen deposition in early IFTA emerge far earlier than detectable fluctuations in filtration markers such as eGFR, leading to missed diagnosis of early occult fibrosis in patients with preserved renal function. Our biochemical-only model achieved an overall AUC of 0.904 but declined to AUC = 0.919 in eGFR ≥ 60 early CKD subgroup, confirming the deficiency of single biochemical modality for early lesion identification. The multi-modal model introduced ASL histogram texture to capture microcirculatory pathological information absent from routine lab tests, maintaining excellent discriminative performance in early CKD populations with preserved eGFR.

4.3 Superior Clinical Feasibility Compared With Other Functional MRI Modalities

Alternative functional MRI techniques including IVIM and BOLD-MRI have been explored for renal fibrosis evaluation[23–25], yet most investigations only utilize averaged diffusion or oxygenation metrics, with limited sensitivity for mild early IFTA. Moreover, IVIM and BOLD sequences impose higher requirements on scanner hardware and patient breath-hold compliance, with inconsistent post-processing standards restricting large-scale clinical promotion. In contrast, our multi-modal model relies on standardized routine biochemistry and widely accessible 3D-pCASL ASL sequences without gadolinium contrast, featuring uniform quantitative post-processing pipelines and superior clinical generalizability.

4.4 Systematic Modeling Framework With Multi-dimensional Validation

We addressed methodological defects of conventional radiomics models through comprehensive optimization in feature screening, anti-overfitting and clinical utility evaluation:Collinearity control[26–28]: Dual diagnostic system combining Pearson heatmap visualization and VIF quantification, with all predictors VIF < 5; Lasso penalization eliminates redundant feature weight while retaining multi-dimensional pathological information;Overfitting prevention: 1000 bootstrap resampling internal validation revealed minimal optimism bias (0.025); non-significant Hosmer-Lemeshow test confirmed excellent model calibration;Clinical value quantification: DCA was introduced beyond simple AUC comparison to quantify net clinical benefit across full risk ranges, covering risk stratification requirements for all outpatient CKD patients;Renal function stratified validation: Subgroup analysis filled the research gap of full-spectrum CKD model applicability, verifying stable discriminative performance in both early and advanced renal impairment subgroups.

4.5 Clinical Translation Potential of the Predictive Nomogram

The proposed predictive model only requires routine renal biochemistry and contrast-free ASL-MRI, without nephrotoxic gadolinium agents, supporting repeated longitudinal follow-up monitoring. The visualized nomogram enables rapid individualized IFTA risk scoring in outpatient clinics to guide stratified intervention strategies.

4.6 Limitations of the Present Study

This research bears two inherent limitations: (1) Single-center prospective cohort without independent multi-center external validation; (2) Absence of long-term clinical endpoint follow-up to validate predictive performance for ESKD progression events. Multi-center external cohorts and longitudinal endpoint tracking will be implemented in future work to further verify generalizability of this model.(3)In addition, the sample size in this single-center prospective cohort was relatively small, with only 37 patients presenting moderate-severe IFTA, which may limit the generalizability of our predictive model. All ASL-MRI examinations were performed on a 3.0T MR scanner; the diagnostic performance of this model may not be directly applicable for 1.5-T systems. Furthermore, histogram feature extraction relied on semi-manual post-processing using 3D-Slicer software and has not been fully automated. Our study cohort mainly enrolled CKD patients who were scheduled for renal biopsy, so caution should be exercised when extrapolating the present model to general outpatient CKD populations without biopsy indications. Multi-center external cohorts and fully-automatic image-processing pipelines will be established in future work to further confirm the robustness and generalizability of this multimodal predictive tool.

5 Conclusions

We developed a nomogram for non-invasive prediction of moderate-severe IFTA by integrating routine renal biochemical markers, mean ASL perfusion and ASL cortical histogram texture features, with rigorous methodological optimization including collinearity correction and Lasso dimensionality reduction, validated comprehensively via ROC analysis, bootstrap calibration, DCA and renal function stratified subgroups. ASL histogram Median and TotalEnergy quantitatively reflect heterogeneous renal cortical perfusion, overcoming the weakness of single averaged RBF values in detecting early focal microvascular injury. Multi-modal fusion integrating biochemical markers and ASL-MRI histogram features yielded numerically higher discriminative performance compared with the biochemical-only model, though the improvement was not statistically significant. The combined model presented favourable calibration and consistent discriminative performance across different CKD renal-function subgroups. This predictive tool supports early screening, serial follow-up and individualized risk stratification of IFTA in CKD patients, with promising clinical translational prospects.

Declarations

Ethics approval and consent to participate

This prospective observational study was approved by the Institutional Review Board of Ningbo Medical Center Lihuili Hospital (Approval No. 2024-IRB-434). The requirement for written informed consent was waived by the IRB because all MRI scans and renal biopsies were routine clinical examinations without additional invasive interventions, and all patient data were fully de-identified before analysis. All procedures were performed in accordance with the 1964 Helsinki Declaration and its amendments.

Consent for publication

Not applicable. No individual-identifiable patient information is included within this manuscript. All images and clinical data have been fully de-identified.

Competing interests

The authors declare that they have no competing interests.

Funding

This study was funded by Natural Science Foundation of Ningbo (Grant No. 2024J426) and the Zhejiang Provincial Health Science and Technology Program (Grant No. 2025HY0870). The funding bodies had no role in study design, data collection, statistical analysis, manuscript writing, or the decision to submit this work for publication.

Author Contribution

Liang: Conceived and designed the study, supervised the research, revised the manuscript, served as the corresponding author;Wu: Patient enrollment, collection of clinical and pathological data;Liu: MRI scanning protocol formulation, image quality control;Shen: Image post-processing, extraction of ASL histogram features;Gan: Statistical analysis, plotting all figures, drafting the original manuscript.

Data Availability

The datasets generated and analysed during the present study are not publicly available due to hospital data protection and patient privacy restrictions, but are available from the corresponding author on reasonable written request with formal ethical approval.

References

1. Yang, C. et al. China Kidney Disease Network Work Group. Executive summary for the China Kidney Disease Network (CK-NET) 2017–2018 Annual Data Report[J]. *Kidney Int.*, **107**(6): 980–984. (2025).

2. Yuan, T. et al. Advancements in the non-invasive diagnosis of renal fibrosis[J]. *Front. Med. (Lausanne)*. **12**, 1646412 (2025).
3. Zhou, H. et al. Effectiveness of functional magnetic resonance imaging for early identification of chronic kidney disease: A systematic review and network meta-analysis[J]. *Eur. J. Radiol.* **160**, 110694 (2023).
4. Poggio, E. D. et al. Systematic Review and Meta-Analysis of Native Kidney Biopsy Complications[J]. *Clin. J. Am. Soc. Nephrol.* **15** (11), 1595–1602 (2020).
5. Copur, S. et al. Future of kidney imaging: Functional magnetic resonance imaging and kidney disease progression[J]. *Eur. J. Clin. Invest.* **52** (5), e13765 (2022).
6. Lafont, T. et al. Advances in biomarkers of acute allograft rejection and interstitial fibrosis/tubular atrophy in kidney transplantation; future perspective and challenges in clinical implementation[J]. *Transpl. Rev. (Orlando)*. **39** (3), 100930 (2025).
7. Fang, W. et al. Three-dimensional pseudo-continuous arterial spin labeling magnetic resonance imaging: an effective imaging technique for early-stage kidney injury in patients with type 2 diabetes[J]. *Quant. Imaging Med. Surg.* **16** (4), 299 (2026).
8. Yuan, G. et al. Noninvasive assessment of renal function and fibrosis in CKD patients using histogram analysis based on diffusion kurtosis imaging[J]. *Jpn J. Radiol.* **41** (2), 180–193 (2023).
9. Addario, G., Moroni, L. & Mota, C. Kidney Fibrosis In Vitro and In Vivo Models: Path Toward Physiologically Relevant Humanized Models[J]. *Adv. Healthc. Mater.* **14** (9), e2403230 (2025).
10. Liu, M. M. et al. Detecting early kidney allograft fibrosis with multi-b-value spectral diffusion MRI[J]. *Sci. Rep.* **15** (1), 40959 (2025).
11. Iatridi, F. et al. KDIGO 2024 Clinical Practice Guideline for the Evaluation and Management of Chronic Kidney Disease in Children and Adults: a commentary from the European Renal Best Practice (ERBP)[J]. *Nephrol. Dial Transpl.* **40** (2), 273–282 (2025).
12. Gu, C. et al. *Multiparametric MR Imaging for Detecting Early Chronic Kidney Disease and Grading Chronic Pathological Changes[J]* (J Magn Reson Imaging, 2026).
13. Loupy, A. et al. The Banff 2019 Kidney Meeting Report (I): Updates on and clarification of criteria for T cell- and antibody-mediated rejection[J]. *Am. J. Transpl.* **20** (9), 2318–2331 (2020).
14. Zhao, Y. Y. et al. Complement 5a receptor 2 attenuates diabetic kidney disease by promoting mitochondria-associated endoplasmic reticulum membrane formation mediated by PSS-MFN2 interaction[J]. *Cell. Discov*. **12** (1), 24 (2026).
15. Malvica, S. et al. Inflammation in areas of fibrosis precedes loss of kidney function in lupus nephritis[J]. *Lupus Sci. Med.* **12** (2), e001687 (2025).
16. Pi, S. et al. Arterial spin labeling and diffusion-weighted MR imaging: quantitative assessment of renal pathological injury in chronic kidney disease[J]. *Abdom. Radiol. (NY)*. **48** (3), 999–1010 (2023).
17. Que, C. et al. An applied study of blood oxygenation level-dependent and arterial spin labeling in early transplant renal function based on renal magnetic resonance angiography examination[J].

Quant. Imaging Med. Surg. **16** (2), 165 (2026).

18. Mao, W. et al. Capability of arterial spin labeling and intravoxel incoherent motion diffusion-weighted imaging to detect early kidney injury in chronic kidney disease[J]. *Eur. Radiol.* **33** (5), 3286–3294 (2023).
19. Ginley, B. et al. Automated Computational Detection of Interstitial Fibrosis, Tubular Atrophy, and Glomerulosclerosis[J]. *J. Am. Soc. Nephrol.* **32** (4), 837–850 (2021).
20. Hu, W. et al. Assessing renal interstitial fibrosis using compartmental, non-compartmental, and model-free diffusion MRI approaches[J]. *Insights Imaging*. **15** (1), 156 (2024).
21. Tampe, D. et al. Different Patterns of Kidney Fibrosis Are Indicative of Injury to Distinct Renal Compartments[J]. Cells, 10(8): 2014. (2021).
22. Wan, S. et al. Noninvasive diagnosis of interstitial fibrosis in chronic kidney disease: a systematic review and meta-analysis[J]. *Ren. Fail.* **46** (2), 2367021 (2024).
23. Srivastava, A. et al. Kidney Functional Magnetic Resonance Imaging and Change in eGFR in Individuals with CKD[J]. *Clin. J. Am. Soc. Nephrol.* **15** (6), 776–783 (2020).
24. Qin, J. et al. Evaluation of Kidney Injury Using Arterial Spin Labeling and Blood Oxygen Level-Dependent MRI: An Experimental Study in Rats With Carbon Tetrachloride-Induced Liver Cirrhosis[J]. *J. Magn. Reson. Imaging*. **60** (5), 2090–2101 (2024).
25. Bane, O. et al. Multiparametric magnetic resonance imaging shows promising results to assess renal transplant dysfunction with fibrosis[J]. *Kidney Int.* **97** (2), 414–420 (2020).
26. Xu, Y. et al. Linking renal hypoxia and oxidative stress in chronic kidney disease: Based on clinical subjects and animal models[J]. *Biomol. Biomed.* **24** (5), 1319–1330 (2024).
27. Li, X. S. et al. Assessment of kidney function in chronic kidney disease by combining diffusion tensor imaging and total kidney volume[J]. *Int. Urol. Nephrol.* **54** (2), 385–393 (2022).
28. Xu, Y. et al. Correlation of Renal Oxygenation with Renal Function in Chronic Kidney Disease: A Preliminary Prospective Study[J]. *Kidney Blood Press. Res.* **48** (1), 175–185 (2023).

Figures

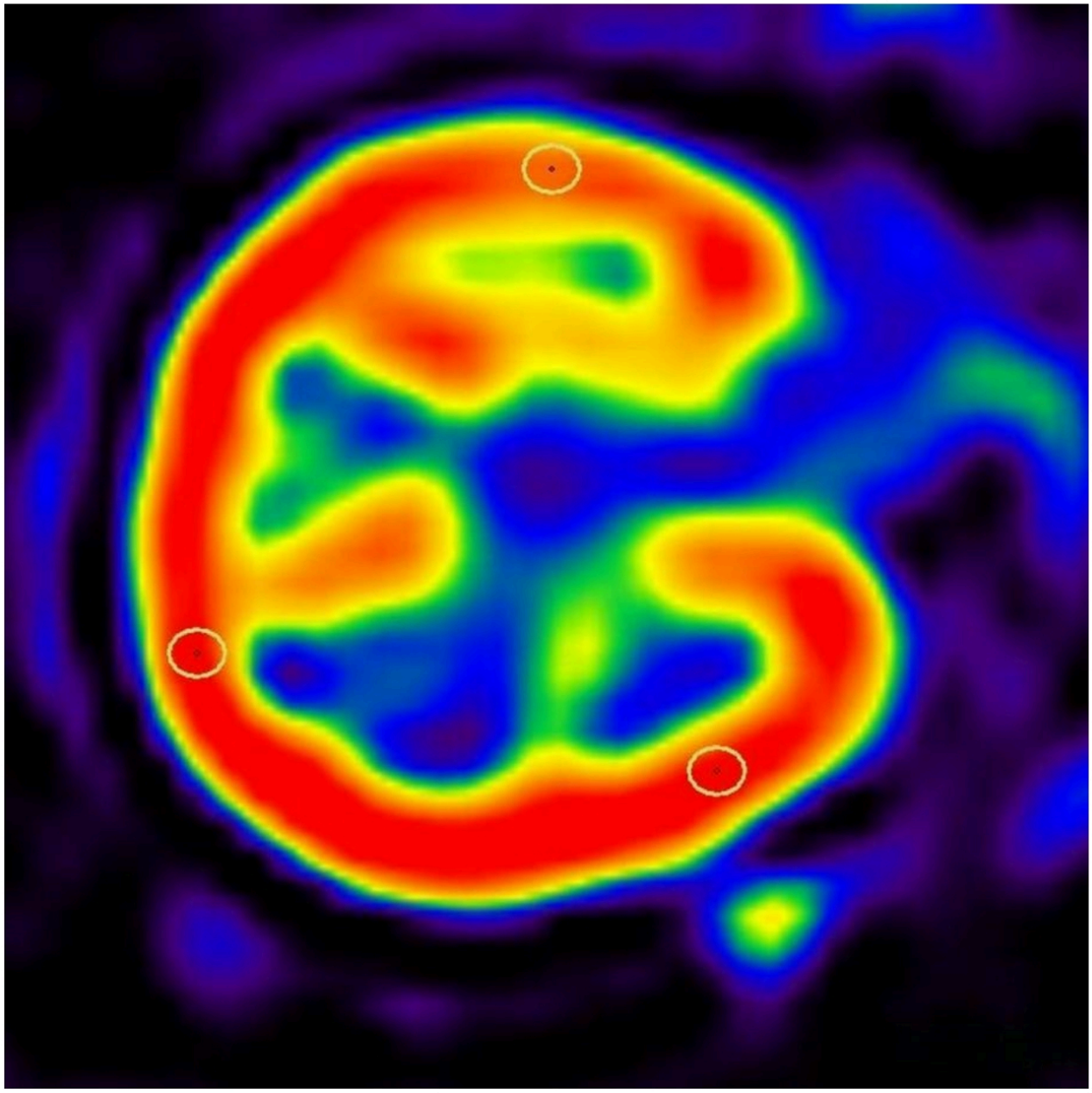


Figure 1

Schematic illustration of ROI placement for renal ASL images

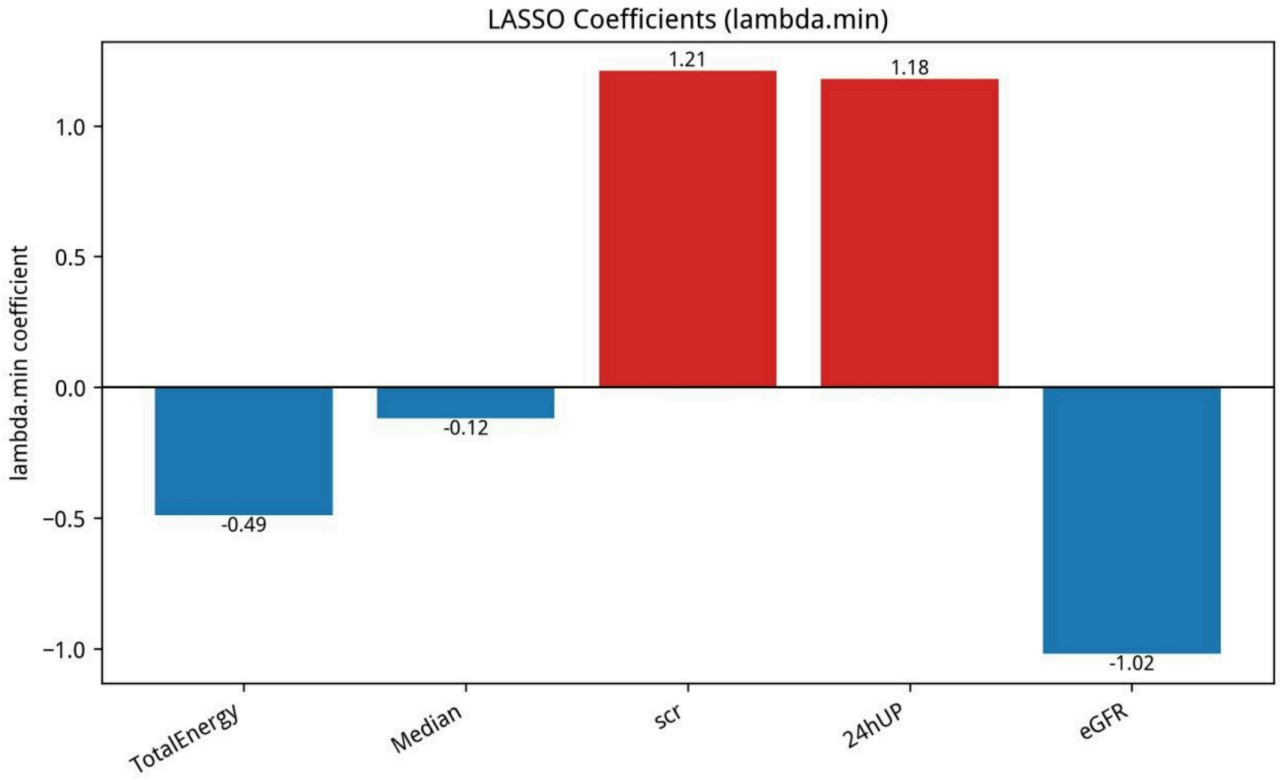


Figure 2

Bar chart of standardized coefficients for each predictor in Lasso regression (optimal penalty coefficient lambda.min)

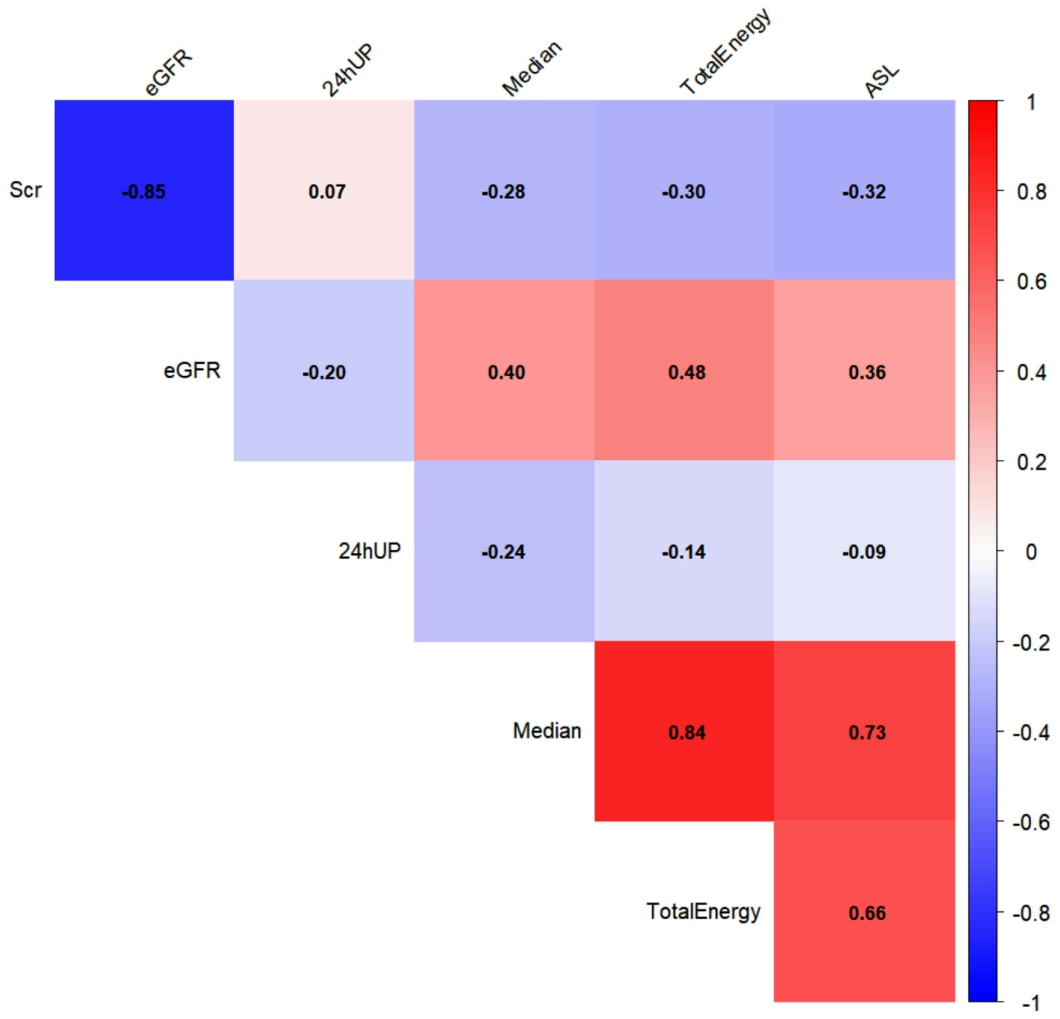


Figure 3

Heatmap of Pearson correlation coefficients for each predictor included in the model

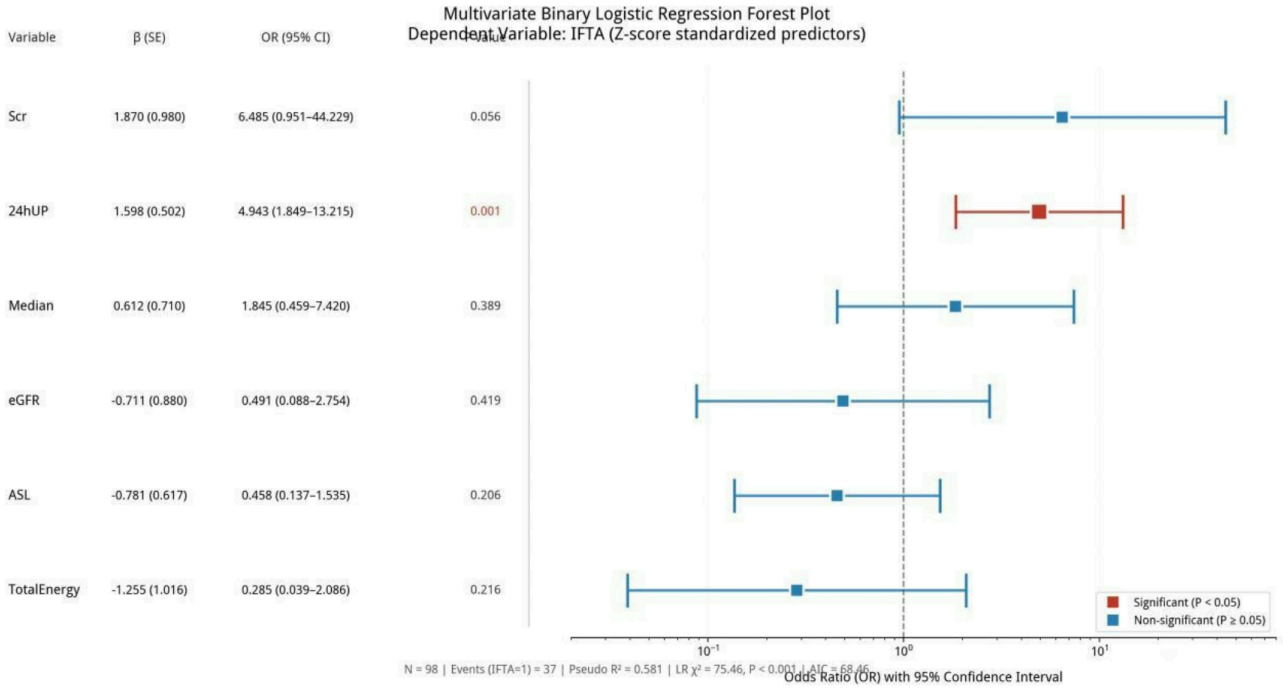


Figure 4

Forest plot of multivariable binary logistic regression for predicting IFTA

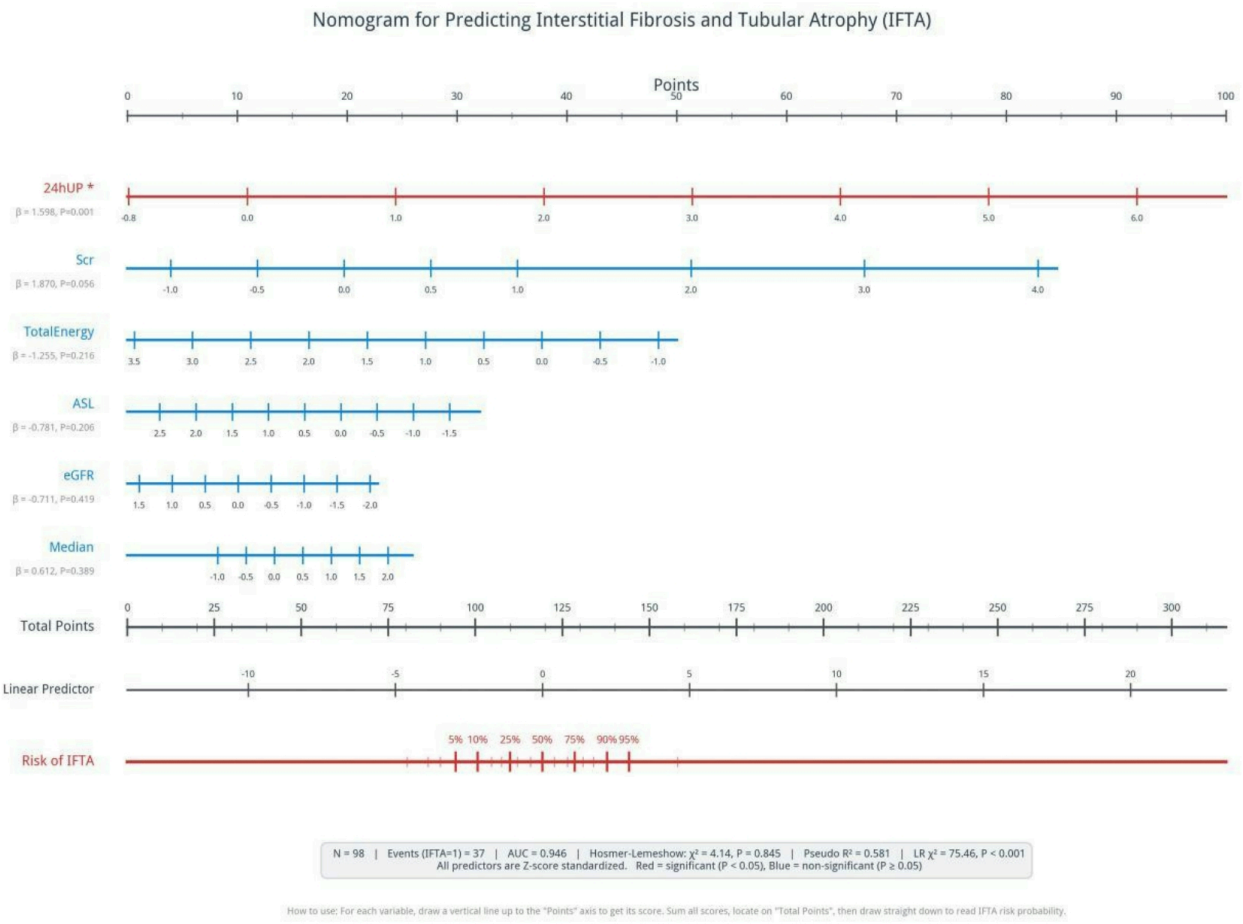


Figure 5

Nomogram for predicting moderate-to-severe IFTA risk based on biochemical and ASL imaging features

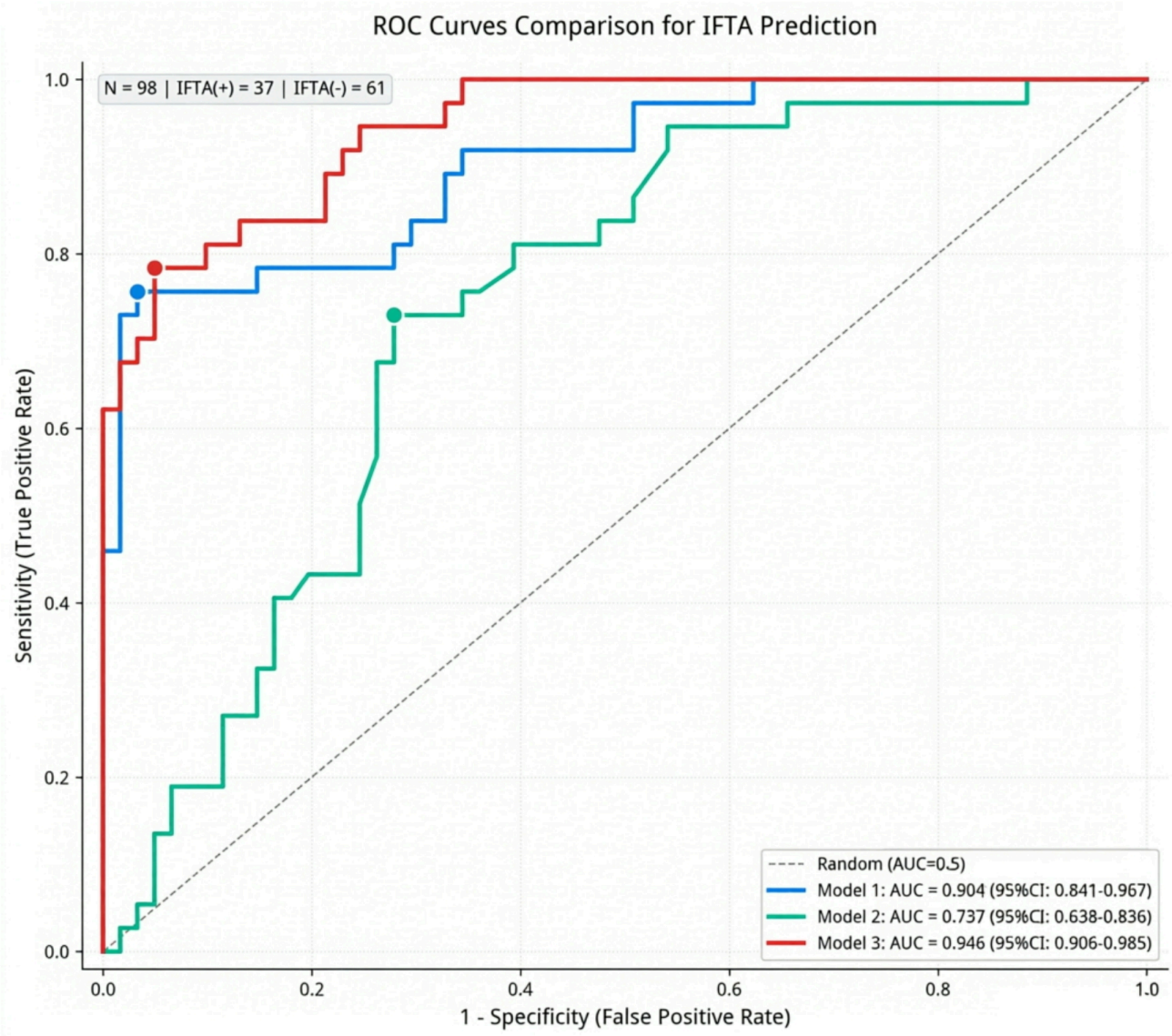


Figure 6

Comparison of ROC curves among the biochemical-only model, the ASL mean perfusion-only model, and the combined biochemical and ASL histogram model

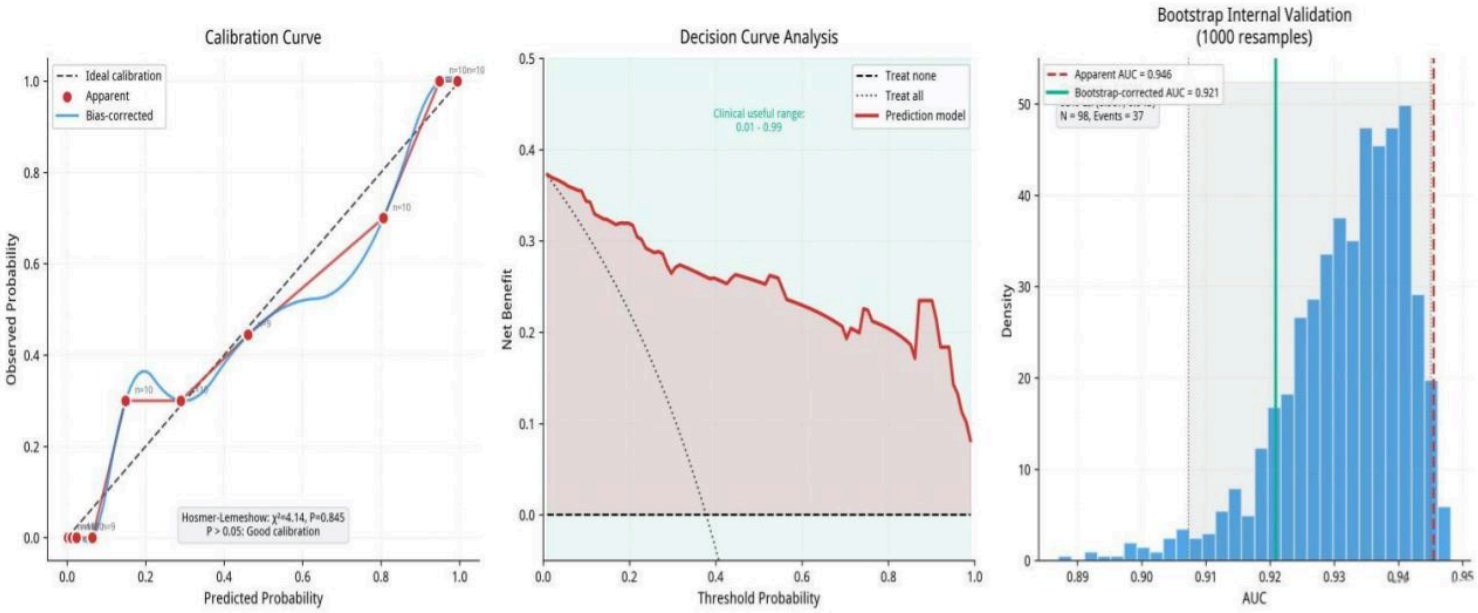


Figure 7

Calibration curve, decision curve analysis, and results of 1000-bootstrap internal validation for the combined model